Critical process temperatures for resistive InGaAsP/InP heterostructures heavily implanted by Fe or Ga ions

André Fekecs[1,4], Martin Chicoine[2,4], Bouraoui Ilahi[1,5], Anthony J. SpringThorpe[3], François Schiettekatte[2,4], Denis Morris[1, 4], Paul G. Charette[1], Richard Arès[1, 4]

[1]*Institut Interdisciplinaire d'Innovation Technologique (3IT), Université de Sherbrooke, Sherbrooke, QC, Canada, J1K 0A5*
[2]*Département de physique, Université de Montréal, Montréal, QC, Canada, H3C 3J7*
[3]*Canadian Photonics Fabrication Centre, NRC, Ottawa, ON, Canada K1A 0R6*
[4]*Regroupement québécois sur les matériaux de pointe, QC, Canada, www.rqmp.ca*

We report on critical ion implantation and rapid thermal annealing (RTA) process temperatures that produce resistive Fe- or Ga-implanted InGaAsP/InP heterostructures. Two InGaAsP/InP heterostructure compositions, with band gap wavelengths of 1.3 µm and 1.57 µm, were processed by ion implantation sequences done at multiple MeV energies and high fluence (10^{15} cm^{-2}). The optimization of the fabrication process was closely related to the implantation temperature which influences the type of implant-induced defect structures. With hot implantation temperatures, at 373 K and 473 K, X-ray diffraction (XRD) revealed that dynamic defect annealing was strong and prevented the amorphization of the InGaAsP layers. These hot-implanted layers were less resistive and RTA could not optimize them systematically in favour of high resistivity. With cold implantation temperatures, at 83 K and even at 300 K, dynamic annealing was minimized. Damage clusters could form and accumulate to produce resistive amorphous-like structures. After recrystallization by RTA, polycrystalline signatures were found on every cold Fe- and Ga-implanted structures. For both ion species, electrical parameters evolved similarly against annealing temperatures, and resistive structures were produced near 500 °C. However, better isolation was obtained with Fe implantation. Differences in sheet resistivities between the two alloy compositions were less than band gap-related effects. These observations, related to damage accumulation and recovery mechanisms, have important implications for the realization ion-implanted resistive layers that can be triggered with near infrared laser pulses and suitable for ultrafast optoelectronics.

Keywords: III-V semiconductors, ion implantation, rapid thermal annealing, crystal defects, Hall effect, X-ray diffraction.

[5]Present address: *Department of Physics and Astronomy, King Saud University, P.O. Box 2455, Riyadh 11451, Saudi Arabia.*

Correspondence to: Prof. Richard Arès
richard.ares@usherbrooke.ca
Fax: 1 (819) 821-7163, Tel: 1 (819) 821-8000 ext. 65012
Département de génie mécanique, 2500 boul. de l'Université,
Université de Sherbrooke, Sherbrooke, QC, Canada J1K 2R1

1. INTRODUCTION

It was demonstrated that ultrafast photoconductive materials based on bulk ternary $In_{0.53}Ga_{0.47}As$ layers can be obtained after Fe ion implantation.[1, 2] Such materials have found their use in novel terahertz spectrometers as photoconductive terahertz sources and detectors working at 1550 nm.[3, 4] The process involves Fe ion implantation done at room temperature with a high ion fluence, close to 10^{15} cm^{-2}, usually followed by rapid thermal annealing (RTA). RTA is aiming at maximizing the on-chip resistivity to enable high external bias for maximum terahertz emission or to minimize thermal noise for sensitive detection. This process was able to achieve apparent electrical resistivity levels up to 80 Ω·cm in Fe-implanted $In_{0.53}Ga_{0.47}As$ layers. [1, 2] Obtaining high resistivity in low band gap InP-related semiconductor compounds (*i.e.*, with $E_g < 1$ eV), using primary ion implantation damage or in presence of secondary damage after annealing, was pointed out to be rather difficult.[5] In these compounds, defects created by implantation tend to pin the Fermi level in the upper half of the band gap. Even though a mid-gap chemical impurity (Fe) was incorporated in these ultrafast materials, their apparent resistivity was much less than what one expects for fully compensated semiconductors. Such "intrinsic" resistivity is strongly dependent on the band gap energy E_g and is about 10^3 Ω·cm at room temperature for the $In_{0.53}Ga_{0.47}As$ alloy ($E_g = 0.74$ eV).[6]

Damage-related isolation studies on the ternary compound $In_{0.53}Ga_{0.47}As$ using Kr^+ and on the quaternary compound InGaAsP using N^+ or He^+ revealed that better resistivity can often be achieved with low implantation temperatures.[7, 8] Comedi *et al.* remarked that amorphization of InGaAsP led to high resistivity and stability after annealing/recrystallization. [8] Similar behaviour was also noted in the case of high fluence Fe implantation studies in $In_{0.53}Ga_{0.47}As$.[6, 9, 10] These observations motivated our use of cold Fe-implantation, done at 83 K, to produce an ultrafast photoconductive material working at 1550 nm which is based instead on an InGaAsP alloy with E_g=0.79 eV. Apparent resistivity levels exceeding 10^3 Ω·cm were achieved.[11]

In this work, we report on a wide range of implantation temperatures (83 K to 473 K) that we investigated in order to obtain resistive Fe-implanted InGaAsP-based materials. We made these investigations by Hall effect measurements. For better insight, we accomplish this with two quaternary alloy compositions lattice-matched to InP (*i.e.*, 1.3Q and 1.57Q). The Q notation represents band gap wavelengths of 1.3 µm and 1.57 µm, respectively. Assuming that intrinsic resistivity levels could be achieved, an increase of the resistivity by a factor of 2-3 was expected with 1.57Q layers over $In_{0.53}Ga_{0.47}As$. A factor of about 50 was expected with 1.3Q layers. These factors take into account the energy gap difference $\Delta E = E_{gQ} - E_{gT}$ between the quaternary and the ternary alloys and are approximated by $e^{\Delta E/0.052}$ (in eV) at room temperature. In order to separate Fe-related deep level contributions from secondary damage contributions, we compare cold implantations made with Fe and Ga ions. We support the interpretations of the results by structural X-ray verifications done after ion implantation and after rapid thermal annealing. Fabrication conditions capable of producing high resistivity levels are then discussed, which gives important insights for developing novel photoconductive InGaAsP-based ultrafast devices.

2. EXPERIMENTAL STUDY

2.1. Fabrication details on ion implanted InGaAsP

InGaAsP/InP heterostructures were grown on 75 mm semi-insulating single crystal (100) InP wafers. They were unintentionally n-doped. This was done by organometallic vapor phase epitaxy (OMVPE) in a multi-wafer reactor (Aixtron). They comprise a quaternary layer of InGaAsP (1.5 µm) capped by InP (0.1 µm) and grown over an InP buffer layer (0.1 µm), as shown by figure 1.

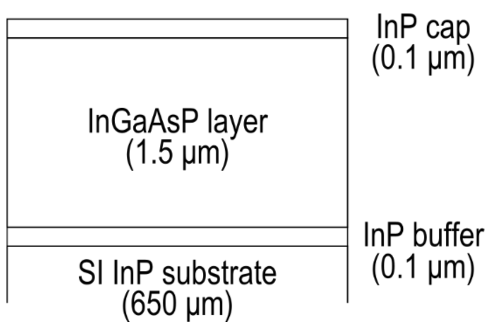

Figure 1. Layer diagram of InGaAsP/InP epitaxial heterostructures used in this work. Nominal thicknesses are indicated for each layer.

A total of four wafers were used, two were grown with a band gap wavelength of 1.57 µm (1.57Q) and the other two had a band gap wavelength around 1.3 µm (1.3Q). Growth temperatures were 625 °C for 1.57Q and 650 °C for 1.3Q. Their properties are reported in

Table I. Photoluminescence (PL) average peak wavelength, substrate lattice mismatch (monitored by X-ray diffraction), as well as molar compositions (x, y) are tabulated for each wafer along with electrical properties determined by Hall effect measurements.

Table 1. List of basic properties of OMVPE grown $In_{1-x}Ga_xAs_yP_{1-y}$/InP structures used in this work. Ion implantation conditions – ion species and implantation temperatures (T_{impl}) – specific to each wafer quarter are also indicated for reference.

Basic properties and implantation conditions	Wafer identification			
	no. 1 E972	no. 2 F697	no. 3 E971	no. 4 F695
PL wavelength (nm)	1565	1575	1309	1341
Mismatch to (004) InP (arc sec)	-240	-380	-220	-320
Composition (x, y)	(0.39, 0.87)	(0.38, 0.86)	(0.27, 0.60)	(0.27, 0.62)
Carrier density (cm^{-3})	2×10^{16}	3×10^{16}	2.4×10^{16}	1.8×10^{16}
Hall mobility ($cm^2V^{-1}s^{-1}$)	3300	2900	2060	1250
Resistivity (Ω cm)	0.09	0.08	0.13	0.28
T_{impl} for ^{56}Fe ions (K)	83, 473	83, 300	83, 373,473	-
T_{impl} for ^{69}Ga ions (K)	-	83	-	83

High fluence, multiple-energy ion implantation was performed at various temperatures (T_{impl}) on InGaAsP wafer quarters (see Table 1). The temperature of the sample holder, a copper block, was controlled by liquid nitrogen and a resistive heater. The pressure in the implant chamber was kept below 1×10^{-6} Torr and samples were tilted at 7° with respect to the ion beam to reduce channelling effects. High energy ions were supplied by a 1.7 MV Tandetron accelerator (High Voltage Engineering Europa). Ion currents from the beam line were of the order of 30 nA. We ran SRIM simulations[12] to develop multiple-energy implantation sequences. Five energies were used and a relative fluence weight was assigned to each in order to produce uniform implant damage and uniform implanted ion density profiles across the InGaAsP layer. The implantation sequence for ^{56}Fe was determined first. The implantation sequence for ^{69}Ga was determined after. Ga is a group III metal already present in the quaternary structure but heavier than Fe, therefore its implantation parameters had to be adjusted to obtain a damage level similar to that of Fe. Other simulation details were given previously.[11] Energies, fluences and profile averages are summarized in Table 2 for both Fe and Ga implantation sequences. Simulated implantation profiles are plotted in figure 2.

Table 2. List of implantation parameters used for high fluence Fe and Ga implantation based on 5-energy profiles SRIM simulations. Averages are calculated over the InGaAsP layer thickness.

Parameters	^{56}Fe implantation sequence	^{69}Ga implantation sequence
Energy (MeV)	(0.25, 0.50, 1.0, 1.8, 2.5)	(0.33, 0.63, 1.15, 2.03, 3.3)
Fluence ($\times 10^{15}$ cm^{-2})	(0.11, 0.22, 0.33, 0.44, 1)	(0.07, 0.12, 0.24, 0.29, 0.74)
Total fluence (cm^{-2})	2.1×10^{15}	1.46×10^{15}
Average density (cm^{-3})	1.1×10^{19}	7.3×10^{18}
Displacements per atom (n_{dpa})	6.5	5.8

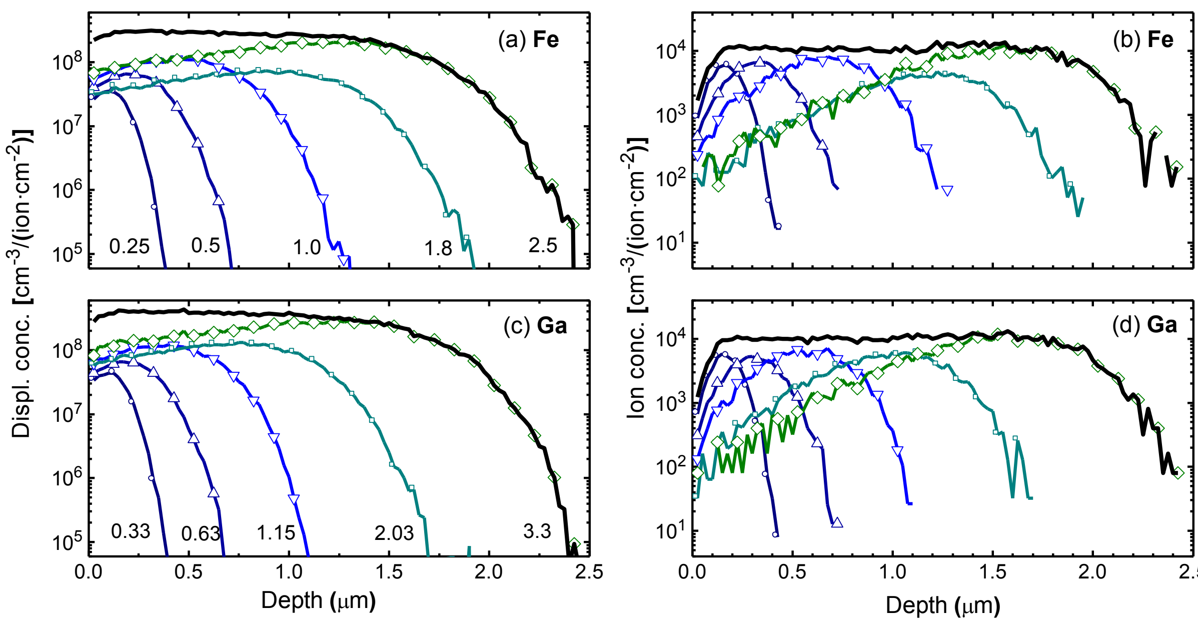

Figure 2. Multiple-energy implantation profiles of the displacement density and the implanted ion density, and their sums, in the InGaAsP/InP structure simulated by SRIM for two heavy ions.(a,b) Fe implantation and (c,d) Ga implantation. Ion energies are indicated in MeV on damage profiles. Details can be found in Table II.

After implantation, surfaces were protected by a resin layer baked at 115 °C. As required, the implanted material was cleaved in 8 mm × 8 mm pieces and the resin was removed in solvents prior to rapid thermal annealing (RTA). The optimization of the annealing temperature was undertaken in steps of 100 °C and sometimes of 50 °C. Each piece was processed at a distinct plateau temperature between 400 °C and 800 °C for 30 s in a dry nitrogen atmosphere using a lamp-based RTA chamber (Jipelec JetFirst). In one instance (Fe-implanted 1.57Q at 300 K) a different RTA apparatus (AG Associates Heatpulse AG610) was employed. Their thermocouple temperature profiles were equivalent. The pieces were placed with their epilayers face down on a clean silicon wafer susceptor. Back chip surfaces were also protected by 10 mm × 10 mm Si proximity caps. Proximity capping with silicon has been described as efficient for protecting InP surfaces from desorption of phosphorous atoms.[13] Each annealed piece was scribed and cleaved down to 6 mm × 6 mm to remove its edges. The final sample was dipped in a solution of HCl to etch selectively the InP cap layer.

2.2. Sample characterization methodology

The structural quality of InGaAsP samples was verified before and after annealing by X-ray diffraction (XRD). High resolution (HRXRD) rocking curves were acquired by an MRD system (PANalytical) equipped with a 4-bounce Ge (220) Bartels monochromator at the source. Edge effects of the line source when surveying small samples were avoided by inserting a square aperture (0.2° × 0.2°) in front of the detector. Rocking curves were also acquired for wide angle scans on an X'pert Pro MRD powder diffractometer (PANalytical) in the Bragg-Brentano geometry equipped with a Xe-filled proportional detector. Electrical properties of the ion implanted InGaAsP thin films were investigated by resistivity and Hall effect measurements at 300 K. Measurements were made in the Van der Pauw geometry on 6 mm × 6 mm samples with indium contacts alloyed at 300 °C for about 75 s. Non-annealed ohmic contacts were formed on as-implanted samples with liquid In-Ga applied at room temperature. The measurements were carried out in the dark and in vacuum, using a commercial Hall system (MMR Technologies, model H-50). Hall voltages were recorded at 0.37 T. The calculations assumed a single carrier type and a unity scattering factor.

3. ION BEAM DAMMAGE

High resolution X-ray diffraction spectra (HRXRD) were taken on as-grown and 1.3Q structures implanted at 3 temperatures (83 K, 373 K and 474 K) with the Fe implantation sequence. Results are shown on Figure 3. The as-grown 1.3Q structure had a double peak signature assigned to the InP substrate (S) and to a quaternary layer (Q). At growth, we aimed for a peak separation of -250 arc sec in order to detect and follow unambiguously the diffraction peak of the modified quaternary layer relative to the (004) reflection peak of the InP substrate. Here, the peak separation (*i.e.,* lattice mismatch) of the as-grown layer corresponded to a slight compressive strain (~0.1 %). A modulation, visible in the tails of the spectrum was produced by interference from the 100 nm InP cap layer.

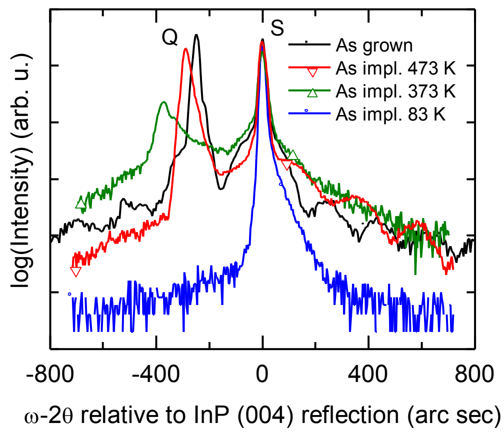

Figure. 3. HRXRD ω-2θ coupled scans taken on a virgin sample of wafer no. 3 (1.3Q) and on samples implanted with the Fe ion sequence at 83 K, 373 K and 473 K. For these measurements, the InP cap layer was still on top of the structure. S=substrate peak, Q=quaternary layer peak.

After cold implantation at 83 K, the diffraction peak of the InGaAsP layer was completely suppressed, leaving out a single diffraction peak assigned to the InP wafer. As a result, long range crystalline order was lost in the quaternary layer. For heavy ions, the nuclear stopping process and the recoil collision cascade produces atom displacements that are clustered in heavily damaged pockets.[14] Multiple-energy implantation distributes them across the quaternary layer. At high enough fluence these pockets accumulate, overlap, and form small amorphous regions. Our work on ion implantation of 1.3Q layers at room temperature has located this onset of amorphization for Fe ions when the average number of displacements par lattice atom (n_{dpa}), simulated by SRIM, was about 0.3. It corresponded to a total fluence of about 4.8×10^{13} cm^{-2}.[15] Here, with the Fe implantation sequence, the simulated n_{dpa} was 6.5 (see figure 2 and Table II) and one reasonably considers the InGaAsP layers as amorphous-like. The simulation showed that n_{dpa} was greater than unity to a depth of 2 μm. Therefore, according to simulations, the top part of the original InP substrate was also amorphized. For greater depths, the total ion damage decayed rapidly; n_{dpa} was less than 0.01 to a depth of about 2.4 μm according to simulations.

We now return to figure 3. Increasing the implantation temperature to 373 K clearly influences the HRXRD spectra; a weak diffraction peak of the quaternary was found to persist. Then at 473 K, the signal from the quaternary layer was almost as strong as in the as-grown material and the modulation from the InP cap layer remained. This lasting effect of the diffracted intensity at 373 K and 473 K was caused by "dynamic defect annealing". The defect annealing occurs during ion implantation and is caused by mobile defects, therefore depends strongly on T_{impl}, the implantation temperature.[14] Dynamic annealing happens on very short time scales and prevents primary heavy ions and recoiling atoms to form heavily damaged pockets and limits damage accumulation. At a critical implantation temperature T_c, the amorphization fluence is, by definition, infinite.[14] T_c is specific to each material and depends on ion species, ion energy and ion flux. At 473 K, the Fe ion implantation of the InGaAsP layer was made close to the critical temperature. Around that temperature, dynamic defect annealing leaves a crystalline material bearing point defects and clusters of point defects.[16]

4. CRITICAL IMPLANTATION AND RTA TEMPERATURES

To obtain resistive InGaAsP/InP heterostructures, we optimized the fabrication process by varying both implantation and RTA temperatures. The efficacy of this optimization was verified against two fabrication parameters: alloy composition (1.3Q and 1.57Q), implantation species (Fe and Ga). Consequently, over 60 samples were produced for this study. To guide our interpretation, structural measurements are presented first.

4.1. Structural verification

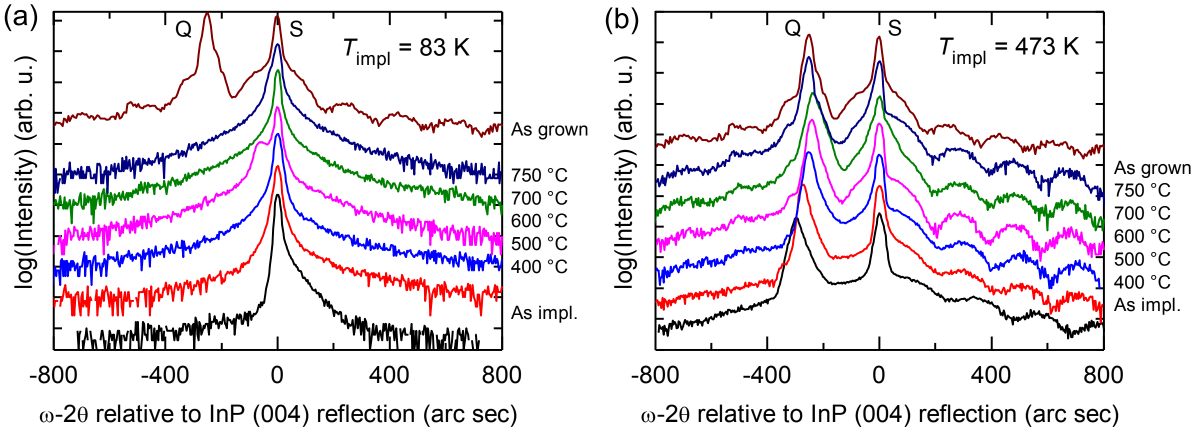

Figure 4. Effect of the RTA temperature on ω-2θ coupled scans. HRXRD spectra taken on a virgin sample from wafer no. 3 (1.3Q) and on samples implanted with the Fe ion sequence at a) 83 K and b) 473 K. S=substrate peak, Q=quaternary layer peak.

HRXRD measurements were taken after RTA for both cold and hot Fe-implanted 1.3Q samples. For samples implanted at 473 K, the RTA temperature had some effects on the shape of the diffraction spectrum shown on figure 4(b). Two narrow peaks were assigned to single-crystal substrate (S) and quaternary layer (Q), respectively. The quaternary layer diffracting angle varied with the RTA temperature which could be the result of the interplay upon annealing between implanted Fe impurities and primary implantation defects. This will be briefly discussed next along with electrical characterization.

For samples implanted at 83 K, the original quaternary layer diffraction signal cannot be recovered for any RTA temperature, as shown by figure 4(a). A secondary defect structure was preventing the detection of a coherent quaternary signal by HRXRD. However, a low angle shoulder was found on one sample, processed with RTA at 600 °C, which could mean that some quaternary domains recrystallized with an orientation that could be detected. Such suppressed diffraction after RTA was observed before with HRXRD studies of cold MeV Fe-implanted $In_{0.53}Ga_{0.47}As$ with a fluence of 5×10^{14} cm^2.[17]

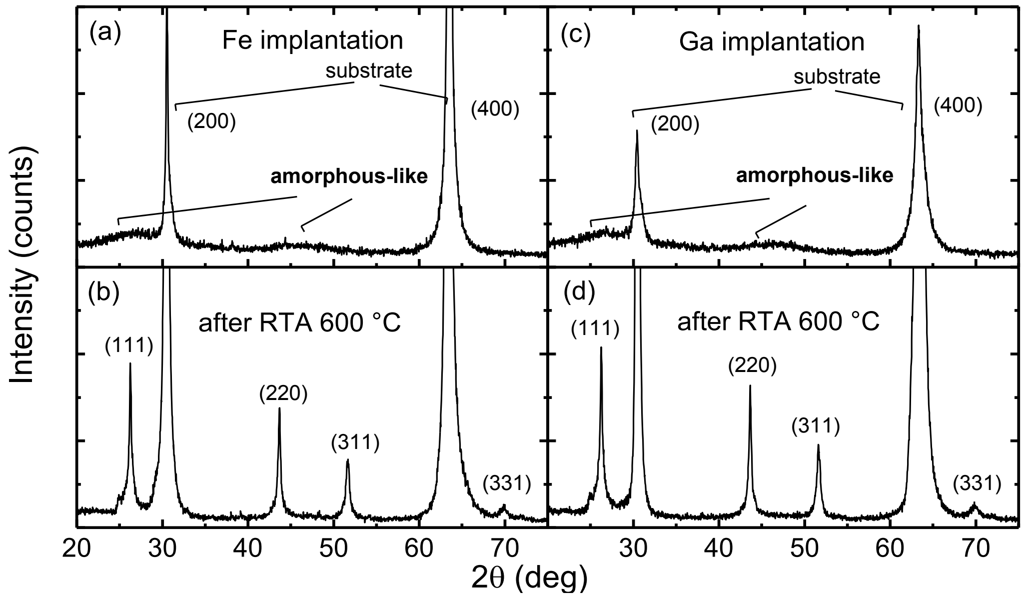

Figure 5. Wide angle XRD ω-2θ coupled scans of cold Fe-implanted and Ga-implanted InGaAsP/InP structures. These comparisons are made for 1.3Q implanted at 83 K. Insets (a) and (c) show diffracted signals from amorphous phases induced by the ion implantation damage. Insets (b) and (d) show diffracted signals from polycrystalline phases obtained after recrystallization by RTA at 600 °C. Strong diffraction peaks from the (001)-oriented InP substrate are also detected, as indicated.

Additional XRD measurements were made at lower resolution using a powder diffraction instrument. Typical wide angle scans recorded for cold as-implanted samples are shown on figure 5(a) and figure 5(c). A weak signal with broad maxima located at 27° and 47° was detected, which corresponds to the signature of a damage-induced amorphous-like phase, as predicted by SRIM simulations in Section 3. The amorphous-like signature was detected in all Fe- and Ga-implanted quaternary materials at T_{impl} = 83 K and 300 K. Several diffraction peaks associated to a cubic zincblende InGaAsP/InP phase were observed on these materials after RTA. This can be seen in figure 5(b) and figure 5(d), which implies the transformation of the amorphous structure into a polycrystalline structure. A polycrystalline structure developed in all quaternary materials Fe- and Ga-implanted at T_{impl} = 83 K and 300 K. The microstructure of this recrystallization have been investigated for Fe-implanted 1.57Q at 83 K, by XRD line profile analysis and electron microscopy, and details are published elsewhere.[18] The findings confirm the full amorphization of the InGaAsP/InP structure up to 1.9 µm below the sample surface. After RTA, multiple structural layers are found. The InGaAsP layer becomes polycrystalline with highly defective submicron grains, a band of planar faults grows at the former amorphous/crystalline interface and a band of secondary extended defects is found at the end-of-range.

4.2. Effects on electrical properties

The optimization of the fabrication process was studied by Hall effect measurements at 300 K. Although great care was taken to obtain uniform ion incorporation and damage density profiles within the InGaAsP layer (figure 2), simulations are predicting profile gradients in the underlying InP substrate and, for cold implantation, an amorphous/crystalline interface. For both hot and cold implantations, distribution of primary and secondary defects may therefore affect a number of layers with different conductivity. Consequently, the Hall measurements most likely consist in a combination of the electrical properties of these layers, not necessarily properties for the implanted InGaAsP layer alone. For that reason, it is better to report about the resistance of these films in terms of sheet resistivity.

Electrical properties produced by Fe implantation in 1.3Q and 1.57Q structures are presented first. These are compared for various implantation temperatures. Data series for dark sheet resistivity, Hall sheet carrier density and effective Hall mobility are plotted against RTA temperatures on figure 6. Data of each sample in the series are shown at its maximum process temperature. Therefore, as-implanted samples equipped with non-annealed In-Ga contacts and equipped with indium contacts are shown at temperature values of 115 °C and 300 °C, respectively. We also show a series of non-implanted 1.3Q reference samples, which had stable electrical parameters upon the whole RTA temperature range, establishing that sample preparation did not create obvious electrical deterioration problems.

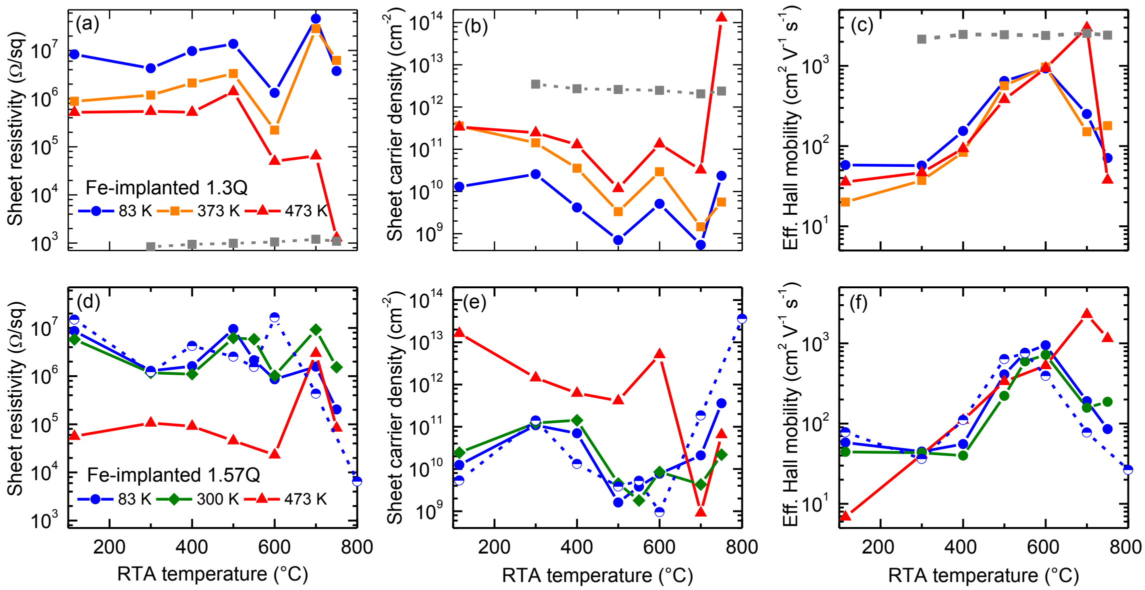

Figure 6. Hall measurements of 1.3Q and 1.57Q structures implanted with the Fe ion sequence showing the effects of the implantation temperature and of the RTA temperature. Insets (a,d), (b,e) and (c,f) show, respectively, dark sheet resistivity, sheet carrier density (n-type) and effective Hall mobility. Dashed grey lines correspond to non-implanted 1.3Q reference samples. Data regarding 1.57Q implanted by Fe at 83 K were published previously and are shown for wafer 1 as a dashed line and for wafer 2 as a solid line.[11]

Compared to cold implantation, hot implantation at 373 K or 473 K resulted in poorer sheet resistivity in 1.3Q and 1.57Q structures. This can be seen in figure 6(a) and 6(d) right after ion implantation and even after annealing, up to 600 °C. A similar trend can be seen also in the sheet carrier density data in figure 6(b) and 6(e). As discussed with the HRXRD data, temperature-driven dynamic defect annealing leaves a crystalline heterostructure bearing Fe impurities and point defects after ion implantation. Such damaged-related centres in ion-implanted InP compounds tend to produce donor levels relatively close to the conduction band.[5, 19] It is also known that, after hot implantation in InP, a large fraction of Fe is activated substitutionally.[20, 21] Therefore, InGaAsP/InP hot-implanted at high ion fluence probably contains a large density of shallow level defects and these appear more abundant than activated Fe-related deep levels and other defect-related deep acceptors. The inspection of carrier density data after RTA suggests that these shallow defects were not annealed efficiently with RTA up to temperatures of 600 °C, probably due to too short annealing times. Kick-out of Fe atoms from substitutional sites due to annealing is another factor that may come into play, as it is the case for long anneals in InP.[20]

This interplay of point defect and substitutional Fe densities probably drove the relative peak location of the InGaAsP layer seen in the HRXRD measurements on figure 4(b). At RTA temperatures around 700 °C, we noticed high resistivity or high effective mobility, but not consistently. This may correspond to an annealing condition where deep Fe-related levels were able to compensate shallow donor defects but confirmation of the interpretation requires further investigation.

With ion implantation done at lower temperatures, *i.e.*, 83 K and 300 K, as-implanted materials had much higher sheet resistivity than with hot implantation. About 10^7 Ω/sq was recorded for both 1.3Q and 1.57Q structures, as shown in figure 6(a) and 6(c). Dependencies to RTA temperature were also comparable for both compositions. Annealing at 300 °C resulted in a small decrease of the resistivity. From 300 °C to 500 °C, a general decline of the sheet carrier density is observed in figure 6(b) and 6(e). A progressive recovery of the effective Hall mobility is observed in figure 6(c) and 6(f), from 300 °C to 600 °C. Maximum resistivity values and minimum carrier densities were achieved between 500 °C and 600 °C. The sheet resistivity increased by more than a 10^4 factor with respect to the as-grown material. The effective Hall mobility peaked generally around 600 °C, close to 10^3 $cm^2V^{-1}s^{-1}$. For RTA temperatures above 600 °C, our results showed a gradual decrease of the mobility. At such temperatures, the carrier compensation process appeared more variable across data series. Some divergences were observed at 700 °C when in some instances the annealed material exhibited high resistivity, a behaviour also reported previously for $In_{0.53}Ga_{0.47}As$ implanted by Fe at 300 K [1] and at 77 K [7].

To help in discriminating possible defect-related effects from Fe-related compensation effects, electrical properties of cold Fe-implanted InGaAsP are compared to Ga-implanted InGaAsP in figure 7. Properties found in as-implanted InGaAsP are discussed first and then, against the RTA temperature.

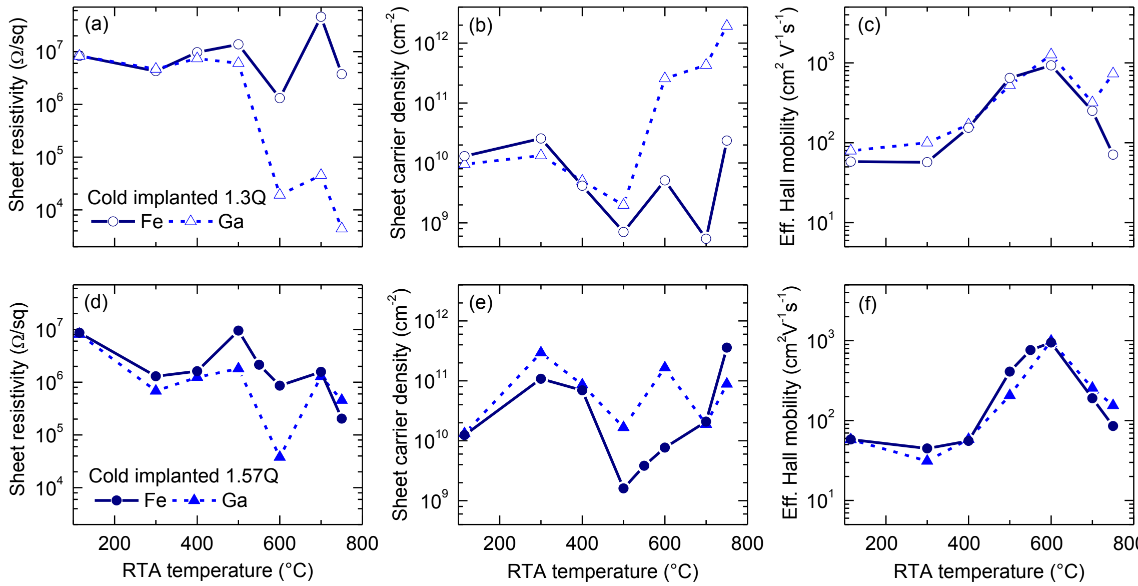

Figure 7. Hall measurements of cold Fe-implanted and Ga-implanted InGaAsP/InP structures after the RTA process. Comparisons for both 1.3Q and 1.57Q implanted at 83 K. Insets (a,d), (b,e), and (c,f) show, respectively, dark sheet resistivity, sheet carrier density (n-type) and effective Hall mobility.

Just after implantation, the Ga ion sequence produced almost identical electrical properties to the Fe ion sequence. We found that InGaAsP/InP structures modified with either cold Fe or Ga implantation have rather high dark resistivity ($\sim 8\times10^{6}$ Ω/sq) and show similar effective carrier density ($\sim 1\times10^{10}$ cm^{-3}). Deep level electrical contributions of Fe did not stand out. We relate this to the same level of primary damage expected from both implantations, which made these materials amorphous-like. It was suggested that amorphous solids can accommodate a locally varying number of covalent bonds, therefore doping impurities are difficult to activate. The carrier compensation effect would rather come from dangling bonds, always present in amorphous semiconductors, which can create deep localized states that usually govern the Fermi level energy.[22] In all cases, effective Hall mobility levels were close to 70 $cm^2V^{-1}s^{-1}$. We suspect that part of conduction within the amorphized layer could be done by carriers thermally excited in extended states rather than by hopping conduction only, since hopping Hall mobility levels are usually much lower.[23] Non-negligible conduction in extended states may be occurring also within the buried layer of the semi-insulating InP substrate that was also ion damaged. This could explain the near-equal resistivity of as-implanted 1.3Q and 1.57Q structures.

After RTA-driven recrystallization, figure 7 shows that above 400 °C cold Fe implantation can produce higher sheet resistivity and lower sheet carrier densities than cold Ga implantation. This suggests a non-negligible contribution to carrier compensation from Fe within at least one of the defective InGaAsP or InP structural layers of the recrystallized heterostructure.[18] However, this contribution occurs at RTA temperatures much lower than those found, and known to be related to Fe activation, using lower, non-amorphizing, Fe implantation fluences in $In_{0.57}Ga0_{.47}As$.[24] On figure 7, sheet carrier density minima are observed around 500 °C and similar effective Hall mobilities are recorded for the whole RTA temperature range up to 700 °C. This common evolution of Hall effect parameters for both Fe and Ga implantation against the RTA temperature may be suggesting the contributions of common post-annealing microstructures or defects. For both Fe and Ga implantation, cold implanted 1.3Q structures were more resistive than 1.57Q structures for annealing temperatures up to 500 °C. However, such difference was not as strong as the bandgap-related effect predicted in the Introduction. Then, for 600 °C anneals, minor differences are observed on the resistivity of both alloy compositions, along with mobility levels which would be exceedingly high for single conduction in a polycrystalline layer. These points, which could be associated to multiple conduction layers or channels, need further investigation.

5. DISCUSSION

The optimization of the fabrication process for high sheet resistivity was closely related to the critical implantation temperature T_c of Fe ions into the InGaAsP layer (Section 3). At T_{impl} = 473 K, strong dynamic defect annealing reduced damage accumulation and prevented amorphization, even if n_{dpa} was ~ 6.5. For implantation temperature of 373 K, the level of dynamic annealing hinted by HRXRD remained significantly large. We conclude that 373 K < T_c < 473 K for MeV Fe ion implantation in InGaAsP. When T_{impl} is close to T_c, the point defect densities left behind by dynamic annealing appeared difficult to remove with RTA. Previous studies made on hot Fe-implanted InP have shown that hour-long high temperature furnace annealing done in phosphorous atmospheres can be more effective to permit high resistivity.[20]

For InGaAsP/InP implanted at 300 K, Hall measurements taken before and after RTA behaved as if the structure was cold-implanted. From these Hall measurements and the wide angle XRD results, we conclude that InGaAsP/InP heterostructures are robust to dynamic annealing at 300 K using our ion implantation process parameters and profiles. According to previous implant damage studies made on binary III-V compounds, the critical implantation temperature T_c is higher in phosphides (for InP and GaP : $T_c \sim 410$ K) than in arsenides (for InAs: $T_c \sim 300$ K, and for GaAs $T_c \sim 340$ K).[25] Since both alloys of the heterostructure (InGaAsP and InP) had high T_c, the Fe ion fluence needed for amorphization would have been similar at 83 K and at 300 K, therefore depths at which crystalline regions are left into the material must be also similar at both temperatures. These depths are dependent to the design of the implantation damage profile (see figure 2 and Section 3).

Compared to previous reports on Fe-implanted $In_{0.53}Ga_{0.47}As$/InP at 300 K, experimental resistivity improvements obtained here with the $In_{0.61}Ga_{0.39}As_{0.87}P_{0.13}$/InP heterostructure were about 13 and 33,[1, 2] which is significant and stronger than what can be expected from a band-gap related effect (*i.e.*, a factor of 2-3 with respect to $In_{0.53}Ga_{0.47}As$, see Introduction). Part of that improvement could be linked to a lower T_c for $In_{0.53}Ga_{0.47}As$, based on data available on InAs and GaAs.[25] Finally, regarding Fe implantation done at 83 K, experimental resistivity improvement factors are smaller, about 4 and 10.[6, 9] In this case, T_{impl} is well below T_c for both alloys. For proper interpretation of this comparison, one will need to investigate further the microstructural effects of the annealing/recrystallization process peculiar to each Fe-implanted heterostructure.

6. SUMMARY AND CONCLUSION

We investigated the fabrication of thin structures made from quaternary InGaAsP alloys grown on InP substrates in order to obtain resistive photoconductive devices that can be triggered with near infrared laser pulses. Critical fabrication process temperatures were found when epitaxial InGaAsP layers underwent high fluence Fe or Ga ion implantation and were subsequently processed by rapid thermal annealing. With hot implantation temperatures (at 373 K and 473 K), dynamic defect annealing prevented the amorphization of the InGaAsP layers. These hot-implanted layers were less resistive and we suspect that the RTA process had difficulty to anneal out implantation induced shallow defects, especially below 700 °C. With cold implantation temperatures, at 83 K and even at 300 K due to the high T_c of the InGaAsP/InP heterostructure, dynamic annealing was minimized and damage clusters could form and accumulate to produce amorphous-like InGaAsP/InP layers. After RTA-driven recrystallization, the use of the Fe ion implantation sequence was better at achieving high sheet resistivity and sheet carrier compensation compared to the Ga ion implantation sequence. Since RTA temperatures near 500 °C were necessary to produce resistive Fe-implanted InGaAsP/InP structures, the material is believed compatible with standard photolithographic and metal deposition process temperatures, which are usually lower, in order to fabricate photoconductive devices for ultrafast optoelectronic applications.

ACKNOWLEDGEMENTS

We want to thank S. Gutierrez, material analyst at the Centre de Caractérisation des Matériaux - CMM (Université de Sherbrooke) for conducting powder XRD measurements. This work was supported by a grant from NSERC through the Canadian Institute for Photonic Innovation. A.F. benefited from a NSERC doctoral scholarship and funding through the Regroupement québécois sur les matériaux de pointe (RQMP). The operation of the Ion Beam Laboratory (Université de Montréal) and the clean room facilities (including RTA equipments at Université de Sherbrooke and INRS-Varennes) were supported by NanoQuébec. We are grateful to CMC Microsystems for facilitating and funding wafer foundry access.

REFERENCES

1. C. Carmody, H. H. Tan, C. Jagadish, A. Gaarder, and S. Marcinkevicius, "Ion-implanted $In_{0.53}Ga_{0.47}As$ for ultrafast optoelectronic applications," *Appl. Phys. Lett.* **82**, 3913 (2003).

2. J. H. Shin, K. H. Park, N. Kim, C. W. Lee, E. D. Shim, Y. C. Kim, D. S. Yee, J. O. Kim, S. J. Lee, and S. K. Noh, "Highly resistive and ultrafast Fe-ion implanted InGaAs for the applications of THz photomixer and photoconductive switch," *AIP Conf. Proc.* **1399**, 935 (2011).

3. M. Suzuki and M. Tonouchi, "Fe-implanted InGaAs terahertz emitters for 1.56 μm wavelength excitation," *Appl. Phys. Lett.* **86**, 51104 (2005).

4. M. Suzuki and M. Tonouchi, "Fe-implanted InGaAs photoconductive terahertz detectors triggered by 1.56 μm femtosecond optical pulses," *Appl. Phys. Lett.* **86**, 163504 (2005).

5. S. J. Pearton and U. K. Chakrabarti, "Ion beam processing of InP and related materials," in *Indium Phosphide and Related Materials: Processing, Technology, and Devices*, edited by A. Katz (Artech House, Boston, 1991), pp. 211-275.

6. S. C. Subramaniam and A. A. Rezazadeh, "The effects of thermal annealing on iron bombarded InP/InGaAs multilayer structures," *Nucl. Instrum. Meth. B* **248**, 59 (2006).

7. P. Too, S. Ahmed, R. Gwilliam, and B. J. Sealy, "Electrical isolation of InP and InGaAs using iron and krypton," *Electron. Lett.* **40**, 1302 (2004).

8. D. Comedi, J. Zhao, K. Jankowska, D. A. Thompson, and J. G. Simmons, "High-resistivity regions in n-type InGaAsP produced by ion bombardment at different temperatures," *J. Appl. Phys.* **76**, 199 (1994).

9. P. Too, S. Ahmed, R. Jakiela, A. Barcz, A. Kozanecki, B. J. Sealy, and R. Gwilliam, "Implant isolation of both n-type InP and InGaAs by iron irradiation: effect of post-implant annealing temperature," in *Electron Devices for Microwave and Optoelectronic Applications, EDMO 2003: The 11th IEEE International Symposium on*, Orlando, FL, 17-18 November 2003, (IEEE, 2003), pp. 18-23.

10. S. Marcinkevicius, C. Carmody, A. Gaarder, H. H. Tan, and C. Jagadish, "Ultrafast carrier dynamics in highly resistive InP and InGaAs produced by ion implantation," in *Proc. SPIE 5352 Ultrafast Phenomena in Semiconductors and Nanostructure Materials VIII*, 26 January 2004, San Jose, CA, edited by K.-T. Tsen, J.-J. Song and H. Jiang (SPIE, 2004), pp. 299-309.

11. A. Fekecs, M. Bernier, D. Morris, M. Chicoine, F. Schiettekatte, P. Charette, and R. Arès, "Fabrication of high resistivity cold-implanted InGaAsP photoconductors for efficient pulsed terahertz devices," *Opt.Mater.Express* **1**, 1165 (2011).

12. J. F. Ziegler and L. U. Biersack J.P., *The Stopping and Range of Ions in Solids* (Pergamon, New York, 1985).

13. A. Quemerais, G. Jezequel, H. L'Haridon, P. N. Favennec, and M. Salvi, "Angle resolved X-ray photoemission study of rapid thermal annealing applied to different GaAs and InP samples," *Electron. Lett*. **26**, 1119 (1990).

14. E. Wendler, "Mechanisms of damage formation in semiconductors," *Nucl. Instrum. Meth. B* **267**, 2680 (2009).

15. A. Fekecs, M. Chicoine, B. Ilahi, F. Schiettekatte, P. G. Charette, and R. Arès, "Towards semi-insulating InGaAsP/InP layers by postgrowth processing using Fe ion implantation and rapid thermal annealing," *J. Phys. D: Appl. Phys*. **46** (16), 165106 (2013).

16. W. Wesch, E. Wendler, and C. S. Schnohr, "Damage evolution and amorphization in semiconductors under ion irradiation," *Nucl. Instrum. Meth. B* **277**, 58 (2012).

17. P. Too, J. Z. Domagala, J. Bak-Misiuk, A. Kozanecki, S. Ahmed, and B. J. Sealy, "Strain and defect structure of iron implanted In0.53Ga 0.47As using high-resolution X-ray diffraction," *Nucl. Instrum. Meth. B* **239**, 414 (2005).

18. A. Fekecs, A. Korinek, M. Chicoine, B. Ilahi, F. Schiettekatte, D. Morris, R. Arès, "Microstructural evolution of a recrystallized Fe-implanted InGaAsP/InP heterostructure," *Phys. Status Solidi A.* doi: 10.1002/pssa.201532006 (2015).

19. C. Carmody, H. H. Tan, and C. Jagadish, "Electrical isolation of n- and p-$In_{0.53}Ga_{0.47}As$ epilayers using ion irradiation," *J. Appl. Phys*. **94**, 6616 (2003).

20. T. Cesca, A. Verna, G. Mattei, A. Gasparotto, B. Fraboni, G. Impellizzeri, and F. Priolo, "Mechanisms for the activation of ion-implanted Fe in InP," *J. Appl. Phys*. **100**, 023539 (2006).

21. K. Bharuth-Ram, W. B. Dlamini, H. Masenda, D. Naidoo, H. P. Gunnlaugsson, G. Weyer, R. Mantovan, T. E. Mølholt, R. Sielemann, S. Ólafsson, G. Langouche, and K. Johnston, "^{57}Fe Mössbauer studies on ^{57}Mn* implanted InP and InAs," *Nucl. Instrum. Meth. B* **272**, 414 (2012).

22. N. F. Mott and E. A. Davis, *Electronic Processes in Non-Crystalline Materials* (Clarendon Press, Oxford, 1979), pp. 42-50.

23. J. Betko, M. Morvic, J. Novak, A. Forster, and P. Kordos, "Hall mobility analysis in low-temperature-grown molecular-beam epitaxial GaAs," *Appl. Phys. Lett*. **69**, 2563-2565 (1996).

24. S. M. Gulwadi, M. V. Rao, A. K. Berry, D. S. Simons, P. H. Chi, and H. B. Dietrich, "Transition metal implants in $In_{0.53}Ga_{0.47}As$," *J. Appl. Phys*. **69**, 4222 (1991).

25. E. Wendler, B. Breeger, C. Schubert, and W. Wesch, "Comparative study of damage production in ion implanted III-V-compounds at temperatures from 20 to 420 K," *Nucl. Instrum. Meth. B* **147**, 155 (1999).